Momentum-distribution spectroscopy using deep inelastic neutron scattering

G. F. Reiter
Physics Department, University of Houston, Houston, Texas

J. Mayers
Rutherford-Appleton Laboratory, Chilton, Didcot, England

J. Noreland
Defence Research Establishment, Stockholm, Sweden

(Received 7 November 2001; published 4 March 2002)

We show that deep inelastic neutron scattering from hydrogen (or other light nuclei) can be used to measure a spectrum of anharmonic contributions to the target atom momentum distribution with high and known accuracy. The method is applied here to determine the momentum distribution of the hydrogen in the hydrogen bonded system KHC_2O_4 (potassium binoxalate), where 23 anharmonic coefficients are obtained at better than the 2σ level. The momentum distribution is obtained to an accuracy of better than few percent at all significant values of momentum.

DOI: 10.1103/PhysRevB.65.104305 PACS number(s): 61.12.−q, 83.85.−c

I. INTRODUCTION

The measurement of proton momentum distributions by neutron scattering is analogous to the measurement of electron momentum distributions by Compton scattering[1] of light and measurement of nucleon form factors by deep inelastic electron scattering.[2] The method is known as neutron compton scattering (NCS) or deep inelastic neutron scattering (DINS). All three techniques rely upon the fact that if the momentum transferred from the incident to target particle is sufficiently large, the impulse approximation (IA) can be used to interpret the data. In the IA, momentum and *kinetic* energy are conserved. From a measurement of the momentum and energy change of the neutron, the momentum of the target nucleus before the collision can be determined.

Because of the requirement of high momentum transfer, DINS measurements have only become practical since the construction of intense accelerator based neutron sources, which have allowed inelastic neutron scattering measurements with energy transfers in the eV region.[3] There have been a few pioneering studies on anisotropic systems at eV energy transfers[4–8] but the analysis has been limited to fitting Gaussians to the observed data, or more generally fitting the data with model containing a few parameters, as was done for measurements on molecular hydrogen.[9] We show here that an entire spectrum of anharmonic coefficients can be measured without recourse to any model, in addition to the widths of an anisotropic Gaussian, thus describing an arbitrary anisotropic and anharmonic momentum distribution in great detail, and providing a sensitive new local probe of the environment of the protons. The possibility of doing this for isotropic systems was first suggested by Reiter and Silver.[10] That possibility, for more general systems, is now a reality. We demonstrate this by measuring the momentum distribution for KHC_2O_4 where we obtain 24 anharmonic coefficients whose size varies by nearly two orders of magnitude, with at least 2-3σ confidence levels for all but one. This system was chosen because it contains an O-H$\cdots$O hydrogen bond in which the proton is located at four sites in the unit cell that are related by reflection symmetry, and hence are equivalent for our purposes, as their momentum distributions are identical. Bonds such as this play a central role in biological systems. It is the anharmonicity of these hydrogen bonds, amongst other things, that determines the configurational changes of complex biological molecules that are essential for their functions, and it is these anharmonicities that are most difficult to calculate accurately. While the measurements we describe cannot provide this information in complex biological molecules, due to the presence of many inequivalent hydrogens, they can provide a database of direct measurements of anharmonicity on simpler systems, with bonds of a variety of strengths, and in a variety of environments. Theoretical calculations and models can be tested and refined on these systems and then used in more complex situations.

The experimental instrument is the EVS spectrometer at ISIS. The work presented here by no means represents the limits of resolution of the instrument, but rather the first experiments of this kind. Upgrades are planned in the near future that will significantly increase flux and counting efficiency.

II. THEORY OF MEASUREMENT

The theoretical basis of neutron Compton scattering is the impulse approximation (IA), which is exact when the momentum transfer and energy transfer are infinite.[11–13] The neutron scattering function $S(\vec{q},\omega)$, is related to the momentum distribution $n(\vec{p})$ in the impulse approximation limit by the relation

$$S(\vec{q},\omega)=\frac{M}{q}\int n(\vec{p})\,\delta(y-\vec{p}\cdot\hat{q})\,d\vec{p}=\frac{M}{q}J(\hat{q},y), \qquad (1)$$

where $y=(M/q)(\omega-q^2/2M)$, M is the mass of the target particle, $q=|\vec{q}|$, and $\hat{q}=\vec{q}/q$.

 ©2002 The American Physical Society

DINS measurements on protons have a particularly simple interpretation, as the interaction of protons with other atoms can usually be accurately accounted for[14–16] in terms of a single particle potential and hence by a proton wave function.[17] From elementary quantum mechanics, $n(\vec{p})$ is related to the Fourier transform of the proton wave function via

$$n(\vec{p}) = \frac{1}{(2\pi)^3)} \left| \int \left| \Psi(r) \exp(i\vec{p}\cdot\vec{r}) d\vec{r} \right|^2 \right. \tag{2}$$

and a DINS measurement of $n(\vec{p})$ can be used to determine the wave function in a way analogous to the determination of real space structure from a diffraction pattern. If $n(\vec{p})$ is known, and if the proton is in a site with reflection symmetry, so that the wave function can be assumed real, then in principle both the proton wave function and the exact form of the potential energy well in which the proton sits can be directly reconstructed.[10] With an asymmetric site such as potassium binoxalate, the phase information that is lost by taking the absolute value of the momentum wave function is irrecoverable, and we will not be able to reconstruct the potential directly. The $n(\vec{p})$ obtained can, of course, be used to check any model potential.

While the original formulation of the inversion problem[10] is complete as it stands, it is useful for the systems we will be dealing with to take into account the anisotropy of the system explicitly. The fundamental result that allows for a simple inversion of the Radon transform $J(\hat{q},y)$ to obtain $n(\vec{p})$ makes use of a basis of Hermite polynomials and spherical harmonics in which the transform is diagonal. That is, a single term in the series for $J(\hat{q},y)$ corresponds to a single term in the expansion of $n(\vec{p})$.

If we express $J(\hat{q},y)$ in this basis as

$$J(\hat{q},y) = \frac{e^{-y^2}}{\pi^{1/2}} \sum_{n,l,m} a_{n,l,m} H_{2n+l}(y) Y_{lm}(\hat{q}) \tag{3}$$

then $n(\vec{p})$ is given in the related basis of Laguerre polynomials as

$$n(\vec{p}) = \frac{e^{-p^2}}{\pi^{3/2}} \sum_{n,l,m} 2^{2n+l} n!(-1)^n a_{n,l,m} p^l L_n^{l+1/2}(p^2) Y_{lm}(\hat{p}), \tag{4}$$

where $\hat{p}$ and $\hat{q}$ are unit vectors. Clearly, since the expansions are complete, a distribution of the form

$$n(\vec{p}) = \prod_i \frac{e^{-p_i^2/2\sigma_i^2}}{(2\pi\sigma_i)^{1/2}} R(\vec{p}) \tag{5}$$

with the σ_i significantly different from each other, could be expanded in this form, but even if $R(\vec{p})$ were 1, it would require a large number of terms in the series. To avoid this, we show that the anisotropy may be taken into account by a change of variables, so that the coefficients $a_{n,l,m}$ represent genuinely anharmonic contributions.

Introducing the new variables

$$p_i' = p_i / \sqrt{2}\sigma_i \tag{6}$$

with $n(\vec{p})$ defined as in Eq. (5), defining $R'(\vec{p}')$ $= R[\vec{p}(\vec{p}')]$, and

$$n'(\vec{p}') = \frac{e^{-p'^2}}{\pi^{3/2}} R'(\vec{p}') \tag{7}$$

we have

$$J(\vec{q},y) = \int n'(\vec{p}')\, \delta(y - \vec{p}'\cdot\vec{q}')\, d\vec{p}', \tag{8}$$

where $q_i' = q_i \sqrt{2}\sigma_i$. The right-hand side of Eq. (8) is no longer a radon transform, since $\vec{q}'$ is not a unit vector. However, defining $y' = y/|\vec{q}'|$ we obtain

$$J(\vec{q},y) = \frac{1}{|\vec{q}'|} \int n'(\vec{p}')\, \delta(y' - \vec{p}'\cdot\hat{q}')\, d\vec{p}' = \frac{1}{|\vec{q}'|} J'(\hat{q}', y'), \tag{9}$$

where $J'(\hat{q}',y')$ is the radon transform of the isotropic (in its Gaussian component) but anharmonic distribution $n'(\vec{p}')$. If $\hat{q}$ is specified as a unit vector in the usual spherical coordinates, then

$$|\vec{q}'| = \sqrt{2}\{[\sigma_1 \sin(\theta)\cos(\phi)]^2 + [\sigma_2 \sin(\theta)\sin(\phi)]^2 + [\sigma_3 \cos(\theta)]^2\}^{1/2}. \tag{10}$$

Our procedure is to expand $J'(\hat{q}',y')$ in hermite polynomials, as in Eq. (3), and least squares fit the data, $S(\vec{q},\omega)$, using Eqs. (1),(9),(10), to obtain the parameters $\sigma_i, a_{n,l,m}$. $n'(\vec{p}')$ can then be reconstructed as in Eq. (4), and we thus obtain $n(\vec{p})$ as in Eq. (5) with $R(\vec{p}) = R'[\vec{p}'(\vec{p})]$. That this is a practical procedure will be demonstrated below.

III. MEASUREMENTS

The measurements were performed on the electron volt spectrometer (EVS),[18] a time-of -flight instrument at the ISIS neutron source. On EVS the final state energy of the scattered neutron is fixed by a resonance filter difference technique.[19] In this technique, a foil, gold in this case, with a sharp nuclear resonance, is alternately inserted and removed from the scattered beam. The two signals are subtracted, leaving only those neutrons that have final state energies within the resonance width remaining in the signal.

The final neutron velocity and energy are related by $E_1 = m\nu_1^2/2$ where m is the neutron mass. The energy of the incident neutron is determined from a measurement of the neutron time of flight via the equation

$$t = \frac{L_0}{\nu_0} + \frac{L_1}{\nu_1}, \tag{11}$$

where t is the measured time of flight, L_0 and L_1 are the lengths of the incident and the scattered flight paths of the neutron, and ν_0 and ν_1 are the speeds of the incident and scattered neutrons. Then

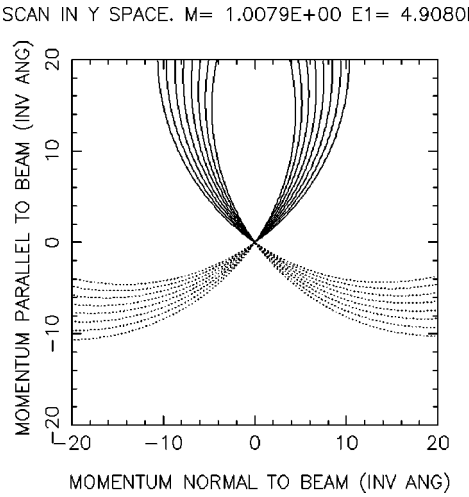

FIG. 1. Scan pattern in momentum space for eight detectors at fixed angles as the time of flight is varied. $E1$ is the resonance energy of the gold foil used in the filter.

$$\hbar\omega = m(\nu_0^2 - \nu_1^2)/2 \tag{12}$$

and

$$\hbar q = m(\nu_0^2 + \nu_1^2 - 2\nu_1\nu_0\cos\theta)^{1/2}, \tag{13}$$

where θ is the scattering angle. From these equations ω and $\vec{q}$ can be determined for a given time of flight t if the instrumental parameters L_0, L_1, θ, and E_1 are known. Hence from the count rate at a given time t, $J(\hat{q},y)$ can be determined. On EVS the detectors are situated in the horizontal plane and hence $\vec{q}$ is always horizontal. By orienting the sample with a chosen crystal axis vertical, it is possible to measure $J(\hat{q},y)$ for $\vec{q}$ in whichever plane, relative to the sample, one chooses. A time of flight scan at a particular angle for a given detector does not correspond, however, to a particular direction of $\vec{q}$. There is significant curvature of this scan through the proton momentum space since the direction of $\vec{q}$ varies significantly over the data region. Time of flight spectra for eight adjacent detectors at angles between 35° and 55° scan through the atomic momentum space of the proton as illustrated in Fig. 1. A complete scan over the proton momentum space is constructed by combining a number of data sets, taken with the sample rotated about the vertical axis by appropriately chosen angles.

The reported measurements were made using two banks of 8 Li^6 doped glass scintillator detectors which were symmetrically placed on each side of the incident beam at scattering angles between 35° and 55°. For DINS studies of protons it is necessary to site the detectors at forward scattering angles since the hydrogen scattering cross section is strongly anisotropic at eV incident energies, with no back scattering. This restriction is a kinematic consequence of the closeness of the mass of the neutron and the hydrogen atom and does not apply to heavier atoms.

The resolution function of the instrument is determined by the uncertainties in the measured values of the time of flight t and the distribution of L_0, L_1, θ, and E_1 values allowed by the instrumental geometry and analyzer foil resolution. Uncertainties in L_0 arise primarily from the finite depth of the neutron moderator, those in L_1 and θ from the finite sample and detector sizes and those in t from jitter in the detector electronics. All resolution components can be determined by calibration measurements and all except the energy component can be approximated by Gaussians, without significant error. A 0.015 mm thick gold foil provided a Lorentzian energy resolution function at $E_1 = 4908$ meV, with a peak HWHM of 136 meV. The Gaussian and Lorentzian resolution components in momentum space y are listed in Table I for two angles representative of the range of angles employed. The resolution is dominated by the energy component which varies strongly with scattering angle. The second most important contribution comes from the angular resolution of the spectrometer and is independent of angle. The momentum and energy transfers at the center of the hydrogen response peak are also listed for the different angles.

TABLE I. The resolution widths are the Lorentzian HWHM for (RL) and the Gaussian standard deviation for other parameters (RG). The momentum q and energy transfer (at the scattering angles 35° and 55° are also given).

Angle	$R_G(\text{Å}^{-1})$	$R_L(\text{Å}^{-1})$	$q(\text{Å}^{-1})$	ω (eV)
35°	0.61	1.08	34.1	2.41
55°	0.55	0.55	48.8	4.92

The raw data contains signals from all the atoms in the scattering sample and from the cryostat background. Fortunately the cross section for hydrogen is much greater than that of other elements and the proton signal is well separated from that due to other masses. The contribution from all components other than hydrogen is subtracted by fitting a sum of Gaussians convoluted with the instrument resolution function to the data and subtracting off the fitted contribution to other peaks. There is also a small contribution to the data from a second gold resonance at 60 eV which can be seen at 100 μsec and this is also fitted and subtracted from the data. The data for each scan was converted into a distribution in the momentum space of the crystal as described above (see Fig. 2). The data has been corrected for sample attenuation, but still contains errors due to small deviations from the impulse approximation which are present at the finite momentum transfers of the measurement. These tend to introduce small asymmetries into the data set for a particular direction, thereby removing the exact inversion symmetry of the Compton profile about the recoil energy (the maximum of the profile). It has been shown by Sears[20] that most of these effects are removed by symmetrization of the data about the recoil energy. There are, however, second order corrections that have even symmetry. The experiments we will describe are precise enough to be sensitive to both sorts of corrections. There is in principle additional information in these corrections that could be used to obtain information about an asymmetric potential. Our procedure is to fit the leading impulse approximation corrections (see Appendix B) along with the coefficients described above, to avoid any

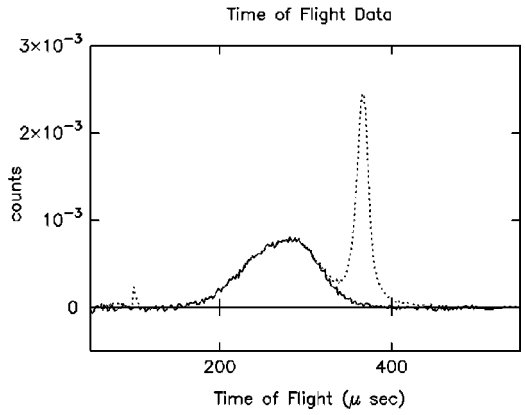

FIG. 2. The sum of data from eight detectors at scattering angles between 38° and 55° is shown as the dotted line. The data after subtraction of the contribution from atoms with higher masses and the 60 eV resonance data is shown as the full line. The total data set for a single plane consisted of 6 spectra as shown in Fig. 1 rotated around the vertical axis by 23° from each other.

contamination of the coefficients describing the momentum distribution, but we make no use of the additional information here.

IV. FITTING PROCEDURES

Equations (3),(4) hold quite generally for radon transform pairs, but physical requirements in the present context restrict the allowed coefficients. Since $J(\vec{q},y)$ is an even function of y, l is restricted to even values, and since $J(\vec{q},y)$ is real, the $a_{n,l,m}$ for $\pm m$ must be equal. As described in Appendix B, the corrections to the impulse approximation include both odd terms in y, which are of order q_c/q, and even terms, of order $(q_c/q)^2$, where $q_c=2\overline{\sigma}/\hbar$ and $\overline{\sigma}$ is an average of the momentum widths.[10] It has a value of approximately 1/8 at the center of the proton response line for the data we will present. The second order corrections are not large but they are measurable, and we will include them in our fitting of the data. These are distinguishable from the even terms in the momentum distribution because of their explicit q dependence, and the fact that q varies with the time of flight in the scans.

For potassium binoxalate, data was taken for three perpendicular planes oriented parallel to the crystal axes The procedure followed was to perform a simultaneous fit to the $6\times16\times3=288$ separate time of flight spectra to an expansion of the form given in Appendix B, Eq. (B1), with $J'(\hat{q}',y')$ defined as in Eq. (9), convoluted with the instrument resolution function.

The data sets as they are presently obtained in the EVS spectrometer at ISIS, are obtained one plane at a time (see discussion of experimental apparatus). That is $\vec{q}$ varies within a plane, and a range of y values is taken such that $J(\vec{q},y)$ is negligible outside this range. There is a very high density of points, which for the purposes of the present discussion we can take to be continuous. The question then arises, ''how many planes of data are needed to determine a specified number of coefficients, and at what angles to each other should they be?'' We can see the point of the question by considering first a single plane and looking at the fit to the leading anharmonic coefficient. From Eq. (3) we see that there are six independent coefficients multiplying H_4, i.e., the coefficients of $(Y_{00},Y_{20},Y_{22},Y_{40},Y_{42},Y_{44})$. Let us say that our coordinate system is chosen so that the plane measured is treated as an xz plane. Then in terms of the variable θ there are only three independent Fourier coefficients that can be present in the data for the coefficients of H_4, i.e., the coefficients of $[1,\cos(2\theta),\cos(4\theta)$, for instance]. Therefore three of the coefficients are not independent. The complete set of coefficients cannot be determined by the data. This is of course due to the fact that there is no information as to the behavior of $J(\vec{q},y)$ for nonzero azimuthal angles ϕ in the data, so we should not expect the fitting procedure to provide it. The data provides a complete description of $J(\vec{q},y)$ only if this function is rotationally invariant about the z axis. Actually, what is required is only that $J'(\hat{q}',y')$ be rotationally invariant, since the fit is done in the primed coordinate system. If this is the case, then all coefficients of Y_{lm} with nonzero values of m must be zero. We see that there are only three remaining possibly nonzero coefficients, which can all be determined. For higher order terms as well, keeping only the coefficients with $m=0$ provides all the independent terms needed to fit the data, and the resulting fit, of course, is rotationally symmetric about the z axis.

If the data is not known to be rotationally symmetric, additional planes of data must be taken to determine even these lowest order coefficients. In general, whenever we take another plane of data, we might expect to obtain three more independent measurements of the coefficients of H_4, four independent measurements of the coefficients of H_6, and in general, $k+1$ measurements of the coefficients of H_{2k}. $(k+1$ being the number of independent Fourier components in the data for that value of k.) Since the number of $a_{n,l,m}$ that are to be determined for $2n+l=2k$ is $(k+2)(k+1)/2$, it appears that $(k+2)/2$ planes are needed to measure all coefficients up to H_{2k}. The angles between the planes must be chosen, however, so that the measurements are really independent. For instance, if $k=2$, it would appear that two planes would suffice, but if they are chosen as the xz and yz planes, they do not provide independent measurements of the coefficients. This may be seen by observing that the sum of the data from the two planes gives three independent Fourier coefficients to determine four independent $a_{n,l,m}$, the coefficients of $(Y_{00},Y_{20},Y_{40},Y_{44})$, since the coefficients of Y_{22} and Y_{42} cannot affect this sum. The difference of the data on the two planes gives three equations for the two coefficients of Y_{22} and Y_{42}. A better choice for the planes would be $\phi=0$ and $\phi=\pi/4$, which would allow the determination of all the coefficients. If there is some symmetry in the problem, one may be able to use perpendicular planes if the symmetry axis is chosen appropriately with respect to the common axis of the two scattering planes. For instance, if there is tetragonal symmetry present, and the symmetry axis is chosen perpendicular to the common axis, one can obtain all the allowed coefficients up to $k=4$. One can show that three perpendicular planes do in fact suffice to determine the co-

efficients up to $k=4$ in the general case, without any symmetry to reduce the number of allowed coefficients. Including the three σ_i, a three plane measurement allows 34 coefficients to be measured if there is no redundancy due to the choice of planes, as we have described above. We find that only the leading corrections to the impulse approximation, as described in Appendix B, are significant in the data. There are in addition, therefore, nine coefficients needed to describe the final state corrections. The coefficients describing these corrections contain additional information, for the case of an asymmetric potential well, beyond that contained in the momentum distribution. We shall not attempt to use that information here to reconstruct the potential, and will not report these coefficients. All of these coefficients may also be obtained with a three plane measurement. The fact that we have about 70 000 data points to fit makes it possible to determine the coefficients with high accuracy.

V. MEASUREMENT ERRORS

The uncertainty in the measurement of $n(\vec{p})$ at some point $\vec{p}$ is due to the uncertainty in the measured coefficients. Denoting an arbitrary coefficient by ρ_i, we have

$$\delta n(\vec{p}) = \sum_i \frac{\delta n(\vec{p})}{\delta \rho_i} \delta \rho_i . \tag{14}$$

The fitting program, after a minimum is obtained with some set of coefficients, calculates the correlation matrix $\langle \delta\rho_i \delta\rho_j \rangle$.[21] Hence, the variance in the momentum distribution is

$$\langle \delta n(\vec{p})^2 \rangle = \sum_{i,j} \frac{\delta n(\vec{p})}{\delta \rho_i} \frac{\delta n(\vec{p})}{\delta \rho_j} \langle \delta\rho_i \delta\rho_j \rangle . \tag{15}$$

There are, of course, potential systematic errors that could enter the measurement, such as multiple scattering effects, or an error in determining the resolution function. The former must be handled with good experimental design, and if small, can be corrected for. We have done measurements on samples whose thickness differed by a factor of 2, with no significant differences in the observed scattering. Multiple scattering effects would also lead to asymmetries in $J(\hat{q},y)$ that are not observed. The resolution function, in so far as it is due to uncertainties in the geometric aspects of the instrument, such as the widths of detectors or the uncertainty in the length of the scattering path, is well known. The shape of the nuclear resonance used in detection, in this case that of gold, is taken to be Lorentzian, which is an approximation. It is also the case, that the resolution varies somewhat with the time of flight, an effect that we neglect by choosing the resolution function over the entire measured momentum distribution to be that at the recoil energy, i.e., the center of the line. This systematic error is the largest one that we are aware of, and is being reduced by the development of more sophisticated software and the overall reduction of the resolution width using double difference techniques and cooled foils. In the present measurement, the resolution width is between 15 and 25 % of the width of the distribution measured. We know from simulations that these systematic errors are substantially smaller than the larger coefficients we measure, but may effect the smaller ones.

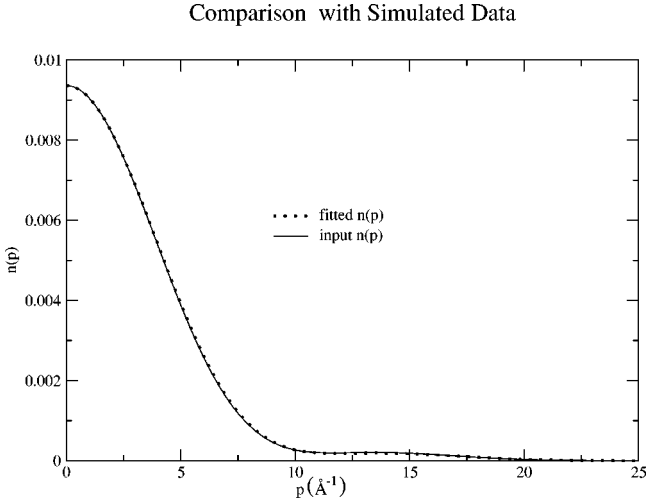

FIG. 3. Comparison of input $n(\vec{p})$, given by Eq. (16) with reconstruction of $n(\vec{p})$ using fitting procedure. The z coordinate axis is chosen to be the double well axis.

A further source of error not contained in the estimate in Eq. (15) is the truncation of the series used to fit the data, which in this case includes only terms up to $2n+l=8$. To get an idea of the seriousness of this approximation, and to test the fitting procedures and software, we have generated synthetic data from a known momentum distribution that corresponds to an asymmetric double well, and convolved it with the assumed instrumental resolution function. The data was then analyzed by the means described above, and the extracted $n(\vec{p})$ compared with the input. The input $n(\vec{p})$ corresponded to a spatial wave function consisting of two displaced Gaussians with the same variance and a relative weight $r=0.5$. The explicit form is

$$n(p_x,p_y,p_z) = \frac{[1+r^2+2r\cos(2p_z a)]}{(1+r^2+2re^{-2a^2\sigma_z^2})} \prod_i \frac{e^{-p_i^2/2\sigma_i^2}}{(2\pi\sigma_i)^{1/2}}, \tag{16}$$

where $\sigma_x=4.6, \sigma_y=4.0, \sigma_z=6.0$, and $a=0.15$ in units of inverse angstroms and angstroms, respectively. This form is similar to the actual form of the data we will analyze. The coordinate system z axis was chosen to be identical with the crystal z axis. The comparison is shown in Figs. 3 and 4. The extracted $n(\vec{p})$ is plotted with a dotted line, the input $n(\vec{p})$ above with a solid line. As may be seen from the figure, there is essentially no error due to the truncation of the the expansion. Of course, an input with more variation might require including higher order terms in the expansion, and hence taking more planes of data. The actual data we have obtained for Potassium Binoxalate has less variation than the simulation and the truncation error will be negligible. In the other directions, the fit is rigorously Gaussian, since all coefficients with $m\neq 0$ were zero. We note that the measured σ_z parameter was 4.47, not 6.0. It is simply a scale parameter. The overall momentum distribution has physical signifi-

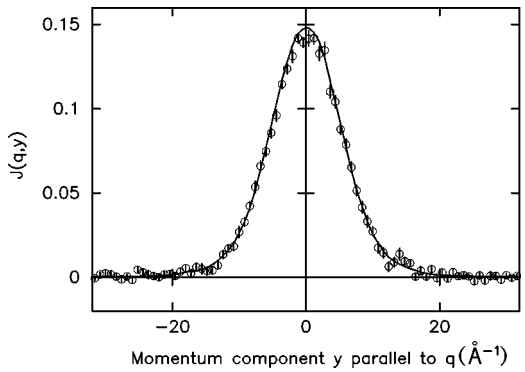

FIG. 4. Data fitted by method described above. The data is a composite of data points in a 10° wedge about the *z* axis.

cance, the individual parameters may not. In fact, we have gotten the same degree of fit with the crystal *z* axis aligned along the coordinate *y* axis. In this case, all the coefficients are nonzero, but the resultant $n(\vec{p})$ is nearly identical to the one displayed above.

A final source of systematic error involves the possibility of finding a false minimum with the fitting procedure. With such a large number of parameters, there is the possibility that the program will home in on a local minimum and miss the true minimum. We are using straightforward gradient methods for the search, which would have difficulty with a very rugged chi-squared landscape. We do not appear to have such a landscape for these problems, and certainly not for the σ_i, or the largest anharmonic coefficients, whose values appear to be quite robust with regards to different paths to the minimum. This possibility is reduced by using a fitting procedure in which the anharmonic coefficients, for fixed values of the nonlinear fitting parameters such as the σ_i, are determined uniquely by linear algebra.[21] This is possible because chi-squared, when one keeps the nonlinear parameters fixed and varies only the coefficients in the series expansion, is a quadratic form in these coefficients. That is

$$\chi^2 = \chi_0^2 - 2\Sigma_i \rho_i B_i + \Sigma_{i,j} A_{i,j} \rho_i \rho_j , \tag{17}$$

where the ρ_i denote a generic coefficient $a_{n,l,m}$, the vector $\vec{B}$ is determined by the data, and the matrix $\underline{A}$ determined entirely by the properties of the instrument. The error matrix defined above is given by the inverse of $\underline{A}$, and can also be obtained by linear algebra, without the need to vary the parameters of the fit.

The nonlinear parameters are then varied, the chi-square minimized with fixed anharmonic coefficients, and the process repeated until it converges. The σ_i then serve as scale factors for the final fit. This procedure also has the advantage that the eigenvalues of the matrix $\underline{A}$ provide a means of eliminating the linear combinations of anharmonic terms to which the instrument is least sensitive, that is, those corresponding to eigenvectors with the smallest eigenvalues.[21] It is also the case, that the eigenvectors are combinations of the fitting functions that are uncorrelated, so that one can eliminate them if there is insufficient signal in the data for a particular eigenvector to be significant, without affecting the quality of the fit with the remaining vectors.

Finally, $n(\vec{p})$ must be positive, and a spurious fit that leads to significant negative values can be rejected. We believe there are no problems of false minimums with the fits we will present.

TABLE II. The scale parameters σ_i and the best fit Gaussian variance $\overline{\sigma_i}$ in each of the three directions.

Harmonic coefficients		
i	σ_i	$\overline{\sigma_i}$
x	5.438	4.017
y	5.757	4.732
z	7.474	5.548

VI. RESULTS FOR POTASSIUM BINOXALATE

Potassium binoxalate KHC_2O_4, is a hydrogen bonded system in which the hydrogen sits in an asymmetric position between two oxygen atoms.[22] The crystal is monoclinic. We will choose a primitive cell for which the bond axis, that is the line joining the two oxygen atoms, is essentially aligned with the *c* axis of the crystal.[23] We choose this axis for the *z* axis of our coordinate system. Three planes of data were taken at right angles to each other, with 69 632 data points in all. One of these is the *bc* plane, where the *b* axis is the unique axis, and the other two are the a^*b and a^*c plane, where the a^* axis is perpendicular to the *bc* plane. These were fit with the methods described above to give the momentum distribution. The measurements were done at 10 K and hence there are no significant finite temperature corrections to the ground state momentum distribution due to excited states.

Note that the coordinate system used to describe the momentum distribution need not have the symmetry of the crystal. The local symmetry of the site is only a twofold rotation. We show the values of the fitted coefficients in Tables II and III, along with the r.m.s. uncertainty in their values. In order to better normalize the coefficients, so that small coefficients correspond to small effects in $n(\vec{p})$, we present $a'_{n,l,m} = a_{n,l,m} 2^{2n+l} n!(-1)^n$. The rms uncertainty in the coefficient is included only to give some sense of the significance of the individual parameters. The error in $n(\vec{p})$ is given by Eq. (14) and includes the effect of the correlations between coefficients, whereas the figures cited in the table are only the diagonal elements of the correlation matrix. It can be seen, that many of the measured coefficients have been determined at the 2–3 σ level of confidence, some at much higher levels, and only one at a 1σ level. Coefficients that are set to zero in the fitting procedure were found to have values smaller than their variance by at least a factor of 2, and setting them to zero did not significantly change the minimum value of chi-square. The goodness of fit to a sample of the data is shown in Fig. 4, where we have compared the fitted prediction, convolved with the instrumental resolution, and the data, for the cumulative sum of data in a

TABLE III. The anharmonic fitting coefficients and their variances as measured.

Anharmonic coefficients				
n	l	m	$a'_{n,l,m}$	$\delta a'_{n,l,m}$
1	0	0	−1.0148	0.0100
0	2	0	−0.1257	0.0072
0	2	2	−0.0350	0.0104
2	0	0	0.0487	0.0074
1	2	0	−0.0365	0.0057
1	2	2	0.1117	0.0163
0	4	0	0.0147	0.0131
0	4	2	0.0364	0.0125
0	4	4	0.0000	0.0000
3	0	0	−0.1134	0.0045
2	2	0	0.0099	0.0018
2	2	2	−0.0436	0.0049
1	4	0	−0.0195	0.0053
1	4	2	0.0359	0.0100
1	4	4	−0.0315	0.0040
0	6	0	0.0140	0.0024
0	6	2	0.0000	0.0000
0	6	4	−0.0856	0.0079
0	6	6	0.0000	0.0000
4	0	0	−0.0025	0.0010
3	2	0	0.0076	0.0005
3	2	2	−0.0038	0.0012
2	4	0	0.0033	0.0010
2	4	2	0.0069	0.0019
2	4	4	0.0000	0.0000
1	6	0	−0.0042	0.0004
1	6	2	0.0000	0.0000
1	6	4	−0.0063	0.0017
1	6	6	0.0000	0.0000
0	8	0	0.0015	0.0006
0	8	2	0.0016	0.0008
0	8	4	0.0032	0.0008
0	8	6	0.0000	0.0000
0	8	8	−0.0139	0.0030

10° wedge along the hydrogen bond direction.

The measured momentum distribution along the bond and perpendicular to it are shown in Figs. 5 and 6. Note that the anisotropy is considerably larger, at nearly all momenta, than the uncertainty in the measurement, for both directions.

In Figs. 7(a), 7(b) we have plotted only the anisotropy in the momentum distribution, that is, the difference between the measured distribution and a best fitting Gaussian whose parameters are given in Table II, and denoted by $\overline{\sigma_i}$. Note that in Fig. 7(a), which is the anharmonicity in the plane perpendicular to the direction of the hydrogen bond, the data are not rotationally invariant about the z axis, and that the x and y axes are not quite equivalent. There is no reason of symmetry for these axes to be equivalent, but if the hydrogen bond were isolated in space, so that the hydrogen felt only the adjoining oxygen ions, the scattering in the x-y plane

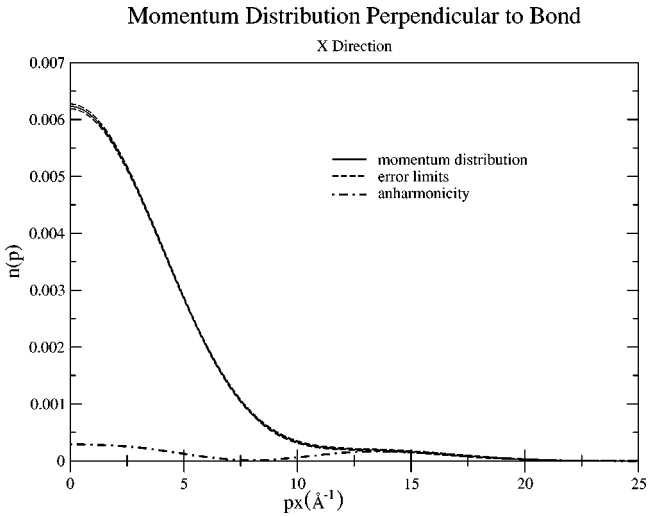

FIG. 5. Momentum distribution for potassium binoxalate perpendicular to the hydrogen bond. The momentum is in units of $Å^{-1}$. The errors are calculated as in Eq. (15) for the parameters that are significant in Table III. The lower curve is the anharmonic component defined as the difference between the measured distribution and the best fitting three dimensional Gaussian distribution.

would be rotationally invariant. The deviations from rotational invariance are due to the effect of surrounding atoms on the bond. We see from the preceding three figures, that the measurements are easily sensitive enough to detect the effects of the environment on the hydrogen bond, even when, as in this case, the anharmonicity is small for all momenta. The coefficients that were measured are given in Tables II and III.

Note that there are 24 anharmonic coefficients that are measurable, 23 of which are at the 2σ level at least, many of which are far more significant.

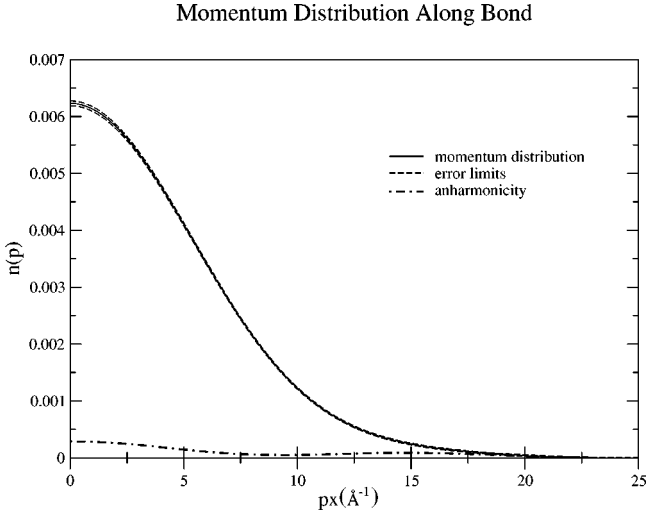

FIG. 6. Momentum distribution for potassium binoxalate along the hydrogen bond. The momentum is in units of $Å^{-1}$. The errors are calculated as in Eq. (15) for the parameters that are significant in Table III. The lower curve is the anharmonic component defined as the difference between the measured distribution and the best fitting three-dimensional Gaussian distribution.

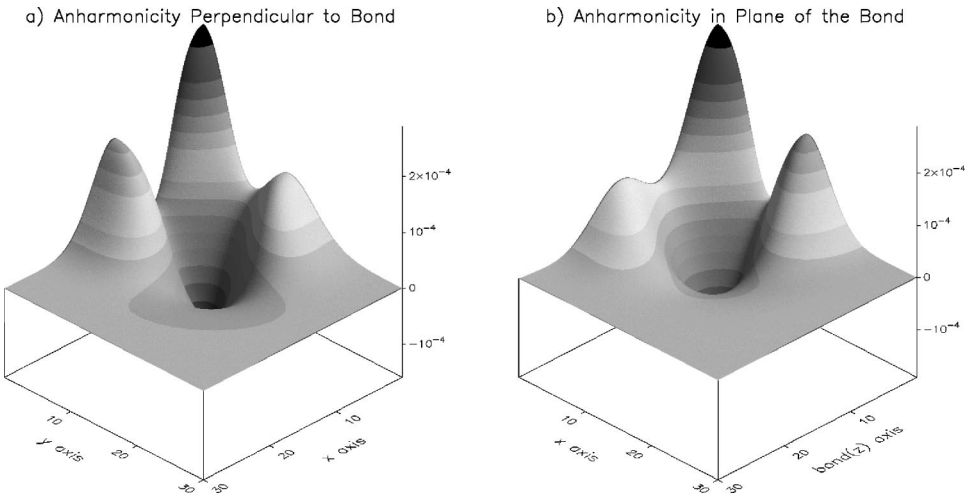

FIG. 7. Anharmonic contribution to the momentum distribution for potassium binoxalate for momenta in the planes shown. The momentum is in units of $Å^{-1}$. The bond axis is the z axis. Note the lack of rotational invariance about the z axis in (a), which is due to the effect of the surrounding ions on the motion of the proton in the bond.

VII. CONCLUSIONS

We have shown how the method of analysis of DINS data suggested in Ref. 10 can be extended to anisotropic momentum distributions, and have applied this method to an analysis of the hydrogen bond in potassium binoxalate. The results demonstrate that DINS, as it is implemented now at ISIS, is capable of detailed, model independent, measurement of the momentum distribution for hydrogen, and by extension, other light atoms. These measurements required about four days of beam time for each plane, and are the first such measurements to be analyzed in this way. The count rates can easily be improved by a factor of ten by adding more detectors, and the resolution can be, and is scheduled to be, significantly improved. The data can be analyzed in less than a day. The DINS technique thus provides a practical means of accessing precise information about the anharmonicity of local potentials and can provide a check of any theoretical calculation of these potentials at a level of accuracy and detail that has not been possible previously. The sensitivity of this distribution to the local environment make it a sensitive new probe of the physical and electronic surroundings of the proton.

ACKNOWLEDGMENTS

We would like to thank Devinder Sivia for assistance in analyzing the data, Steve Bennington and John Tomkinson for useful discussions, and Professors R. G. Delaplane and H. Kuppers for providing the crystals.

APPENDIX A: SEPARABLE DISTRIBUTIONS

The distribution used for the simulations described here is a special case of a general separable distribution

$$n(\vec{p}) = \prod_i n_i(p_i). \tag{A1}$$

If we represent

$$n_i(p_i) = \frac{e^{-p_i^2/2\sigma_i^2}}{(2\pi\sigma_i)^{1/2}} \sum_n a_{i,n} H_n\left(\frac{p_i}{\sqrt{2}\sigma_i}\right), \tag{A2}$$

make use of the fact that

$$\int e^{iqx-x^2} H_n(x)\,dx = \pi^{1/2} e^{-q^2/4} (iq)^n, \tag{A3}$$

and represent the delta function in the definition of the radon transform by its Fourier transform, it is straightforward to show that the radon transform of $n(\vec{p})$ in the isotropic coordinate system defined in the text is given by

$$J'(\hat{q}',y') = \frac{e^{-y'^2}}{\pi^{1/2}} \sum_{n_j} \left[\prod_i a_{i,n_j}\left(\frac{q_i'}{q'}\right)^{n_j}\right] H_{n_1+n_2+n_3}(y'). \tag{A4}$$

For the case we have used as a simulation, in which the distribution is anharmonic only in the z direction, the result simplifies to

$$J'(\hat{q}',y') = \frac{e^{-y'^2}}{\pi^{1/2}} \sum_n a_{3,n}[\cos(\theta')^n] H_n(y'). \tag{A5}$$

In this case, the coefficients in the expansion of $J'(\hat{q}',y')$ in the form given by Eq. (3) are not all independent. There is only one independent coefficient in the set of $a_{n,l,0}$ for each value of $2n+l$.

APPENDIX B: FINAL STATE CORRECTIONS

We give here the extension of the results of Sears[12] on the final state corrections to the impulse approximation to the case of anisotropic momentum distributions. The derivation is straightfroward, and need not be given here. The vector $\vec{q}'$ is defined here as $q_i' = \sqrt{2} q_i \sigma_i$. The leading terms in $1/q$ and in the number of spatial derivatives taken are

$$S(\vec{q},\omega)=\frac{M}{q'}\Bigg\{J'(\hat{q}',y')$$
$$-\sum_{i,j} q_i q_j \left\langle \frac{\delta^2 V}{\delta x_i \delta x_j}\right\rangle \frac{\delta^3 J'(\hat{q}',y')}{\delta^3 y'}\frac{\hbar M}{12q'^3}$$
$$+\sum_{i,j} q_i q_j \left\langle \frac{\delta V}{\delta x_i}\frac{\delta V}{\delta x_j}\right\rangle \frac{\delta^4 J'(\hat{q}',y')}{\delta^4 y'}\frac{M^2}{24q'^4}$$
$$+\sum_{i,j,k,l} q_i q_j q_k q_l \Bigg[A_{i,j,k,l}\frac{\delta^5 J'(\hat{q}',y')}{\delta^5 y'}\frac{1}{5!q'^5}$$
$$+S_{i,j,k,l}\frac{\delta^6 J'(\hat{q}',y')}{\delta^6 y'}\frac{1}{6!q'^6}\Bigg]\Bigg\}. \quad \text{(B1)}$$

The tensors $S_{i,j,k,l}$ and $A_{i,j,k,l}$ can be expressed[12] in terms of averages of combinations of derivatives of the potential and products of the momenta. Since we will make no use of the explicit form of these tensors, and they are quite complicated, we will not give these expressions here.

In principle, for symmetric potentials, the potential itself is determined by the momentum distribution, so one could determine the averages appearing in Eq. (B1) by an iterative process, and there would be no additional parameters to fit. However, in the present case where the potential is asymmetric, or more generally, where the final state effects include many-particle corrections, one must fit these averages as well. Since $S(\vec{q},\omega)$ is even in q, the quadratic terms in q can be represented as a sum of the three even spherical harmonics up to $l=2$. The quartic terms can similiarly be represented by the six even spherical harmonics up to $l=4$. The inclusion of these terms in the fit is simplified by the fact that

$$\frac{\delta}{\delta y}e^{-y^2}H_n(y)=-e^{-y^2}H_{n+1}(y) \quad \text{(B2)}$$

so that, for instance, the leading correction term in Eq. (B1) consists of a series with the same coefficients as in Eq. (3), but with $H_{2n+l}(y)$ replaced by $H_{2n+l+3}(y)$. The fitted terms from the final state corrections provide the possibility of access to some information on the antisymmetric part of the potential.

The appearence of even Hermite polynomials in the $1/q^2$ final state correction raises the question of whether they can be separated from the even polynomials in the expansion of $J'(\hat{q}',y')$. This would not be possible for data taken at constant q, but for the time of flight data, where the value of q varies significantly for each individual time of flight scan, the functional form of the the two sets of terms on the dataset is quite different, and they can be readily distinguished from each other.

Since we will make no use of the averages of the potential, we will not try to extract them from the data. And, since our data is not very strongly anharmonic, we will keep in the expansion of Eq. (B3) the terms that correspond to derivatives of the leading Gaussian term only, and that only for the first two corrections to the leading impulse approximation term. That is terms of the form $H_3(y)/q$ and $H_4(y)/q^2$ with the appropriate angular dependent factors.

[1] P.M. Platzmann, in *Momentum Distributions*, edited by R.N. Silver and P.E. Sokol (Plenum Press, New York, 1989), p. 249.
[2] I. Sick, in *Momentum Distributions* (Ref. 1), p. 175.
[3] R.S. Holt, J. Mayers, and A.D. Taylor, in *Momentum Distributions* (Ref. 1), p. 295.
[4] H. Rauh and N. Watanabe, Phys. Lett. **100A**, 244 (1984).
[5] M.P. Paoli and R.S. Holt, J. Phys. C **21**, 3633 (1988).
[6] S. Ikeda, K. Shibata, Y. Nakai, and P.W. Stephens, J. Phys. Soc. Jpn. **61**, 2619 (1992).
[7] P. Postorino, F. Fillaux, J. Mayers, J. Tomkinson, and R.S. Holt, J. Chem. Phys. **94**, 4411 (1992).
[8] A.L. Fielding, D.N. Timms, and J. Mayers, Europhys. Lett. **44**, 255 (1998).
[9] J. Mayers, Phys. Rev. Lett. **71**, 1553 (1993).
[10] G. Reiter and R. Silver, Phys. Rev. Lett. **54**, 1047 (1985).
[11] R. Newton, *Scattering Theory of Waves and Particles* (Springer, Berlin, 1981).
[12] V.F. Sears, Phys. Rev. B **30**, 44 (1984).
[13] J. Mayers, Phys. Rev. B **41**, 41 (1991).
[14] S.W. Lovesey, *Theory of Neutron Scattering from Condensed Matter* (Oxford University Press, New York, 1987).
[15] R. Hempelmann, D. Richter, and D.L. Price, Phys. Rev. Lett. **58**, 1016 (1987).
[16] M. Warner, S.W. Lovesey, and J. Smith, Z. Phys. B: Condens. Matter **39**, 2022 (1989).
[17] This assumes that the temperature is sufficiently low that the proton is essentially in its ground state. This condition is well satisfied for the experiments we will discuss.
[18] J. Mayers and A.C. Evans (unpublished).
[19] P.A. Seeger, A.D. Taylor, and R.M. Brugger, Nucl. Instrum. Methods Phys. Res. A **240**, 98 (1985).
[20] V.F. Sears, Phys. Rev. **185**, 200 (1969); Phys. Rev. A **7**, 340 (1973).
[21] D. Sivia, *Data Analysis: A Bayesian Tutorial* (Clarendon Press, Oxford, 1996).
[22] H. Einspahr, R.E. Marsh, and J. Donohue, Acta Crystallogr., Sect. B: Struct. Crystallogr. Cryst. Chem. **28**, 2194 (1972).
[23] This choice differs from the choice in the previous reference, and corresponds to choice 3 for the unit cell of crystal type 14 with the *b* axis the unique axis in the standard tables, *International Tables for Crystallography* (Riedel, Dordrecht, 1983), Vol. A, p. 177.